Induced seismicity in the Reykjanes geothermal reservoir, Iceland: seismic event monitoring, characterization and clustering

Laure Duboeuf[1], Volker Oye[1], Inga Berre[2] and Eirik Keilegavlen[2]

[1] NORSAR, Gunnar Randers vei 15, Kjeller, Norway

[2] University of Bergen, Bergen, Norway

laure@norsar.no

Keywords: Induced Seismicity, Fractures, Clustering, Geothermal Reservoir, Fluid Injections, Reykjanes

ABSTRACT

Identification of reactivated geological structures related to fluid flow is a crucial goal to mitigate damages related to fluid injections in geothermal systems and optimize production. This study focuses on three weeks of seismicity, recorded by a dense surface network of 38 stations in 2015, in the Reykjanes geothermal field (SW of Iceland). We expect to map the fractures through the combination of two techniques based on cross-correlations: a double-difference relative location and an event clustering using a multiplet analysis. Among 1800 detected events, 626 are suspected to be induced and were absolutely located. They were characterized by a low frequency content (from 2 to 30 Hz) and moment magnitudes varying between -0.8 and 2.8. Of the events, 537 could be relocated (REs) and are found to be within or close to the geothermal fields. The 89 remaining seismic events, which only have an absolute location (NREs), surround the geothermal plant locations and are the biggest events (Mw > 1). This different location pattern between REs and NREs leads us to suspect a different control of the triggering: REs might be induced and NREs natural events. In addition, 233 events were gathered into 9 clusters and analyzed in function of the time. This might allow the identification of potential vertical fractures and a subset of inclined parallel fractures.

1. INTRODUCTION

Induced and triggered seismicity related to subsurface processes at geothermal power plants is an active field of research (Albaric et al., 2014; Brodsky & Lajoie, 2013; Cuenot et al., 2008; Kwiatek et al., 2015; Shapiro et al., 1999; Zhang et al., 2017). Occurrence of seismic events has been observed and studied in various geothermal fields around the world, as for example in Soultz-sous-Forêts, France (Cornet et al., 2007; Schmittbuhl et al., 2014), in the Geysers, USA (Martínez-Garzón et al., 2013), in Brawley, USA (Wei et al., 2015) or again in Reykjanes, Iceland (Jousset et al., 2016; Weemstra et al., 2016). Often, the seismic activity is directly related to the fluid injection periods (Cornet et al., 1997; Shapiro et al., 2002). However, at several sites, even some of the larger events have occurred after the end of injections, as the M_L 3.2 Basel event (Zang et al., 2017; Bachmann et al., 2011; Cornet, 2016; Deichmann & Giardini, 2009). Understanding the link between fluids and induced seismicity as well as being able to identify which fractures might be reactivated are crucial for a stable operation of geothermal power plants (EGS and conventional) and are also important with respect to earthquake hazard and risk assessment.

In the past, seismicity induced by fluid injections has already been used to perform detailed fracture mappings (Fehler et al., 2001; Li et al., 1998; Michelet & Toksöz, 2007; Phillips et al., 1997; Rowe et al., 2002). Thus, Michelet and Toksök (2007) mapped the induced fractures only using event locations in the Soultz-sous-Forêts geothermal field (France). Their main emphasis was to reduce the event location uncertainty by combining techniques: joint hypocenter location and multiplet analysis. This allows precise relocation (within 10 m) as well as characterization of events, which occurred along fractures.

Our study focuses on the seismicity recorded in the Reykjanes Peninsula (South-West of Iceland, Figure 1) from the 20th of May 2015 until the 14th of August 2015. After we applied an automated event detection algorithm for this period, we focused our interest on analysis and interpretation of three weeks of seismicity. In the following steps, we first conduct an absolute event location, followed by a relative event relocation. Not all events have been relocated, because some pre-conditions, like the distance between event pairs, need to be fulfilled to allow for relocation. Therefore, we end up with a family of events that are relocated and another family of non-relocated events. For all events, we conduct a clustering analysis. Then, we compare the difference between relocated and non-relocated events, clustered and non-clustered events, and location and magnitude of events. This leads us to identify some distinct seismic signatures. Finally, we restrain spatially and temporally our study to the Reykjanes Geothermal field during the week 30 of 2015. We further analyze the origin time of the seismic events with respect to their locations. We also analyze clustering, magnitude and distance to the injection

point to interpret potential relations to fluid flow parameters and geological patterns.

2. GEOLOGICAL AND SEISMO-TECTONIC SETTINGS AND FLUID INJECTION PROPERTIES

2.1 Geological/tectonic settings

The study area, i.e. the Reykjanes Geothermal System, is located at the South-West of the Reykjanes Peninsula, in Iceland (Figure 1), in a complex geological system. In fact, the North Atlantic Ridge goes right through the Reykjanes Peninsula, which is in addition positioned above a hot spot. Hence, Iceland is both an active seismic and volcanic zone (Björnsson & Einarsson, 1974; Jakobsdóttir, 2008; Thordarson & Larsen, 2007).

The Reykjanes peninsula is composed of young magmatic rocks (<0.8 Ma). First, on the top, postglacial Holocene lava layers, whose ages vary from the 13th century to 0.015 Ma, reach down to about 400 m depth. Below those, older lava series and altered sediments are observed, from 400 to 1200 m depth. Then, down to 3000 m depth, a sequence of pillow lava has been identified. The volcanic activity in this area also results in an unusual high temperature. The temperature is of 320°C at 3 km depth and reaches 427 °C at 4.6 km into the Reykjanes Peninsula (Khodayar et al., 2018). This is one of the reasons to exploit the geothermal energy here.

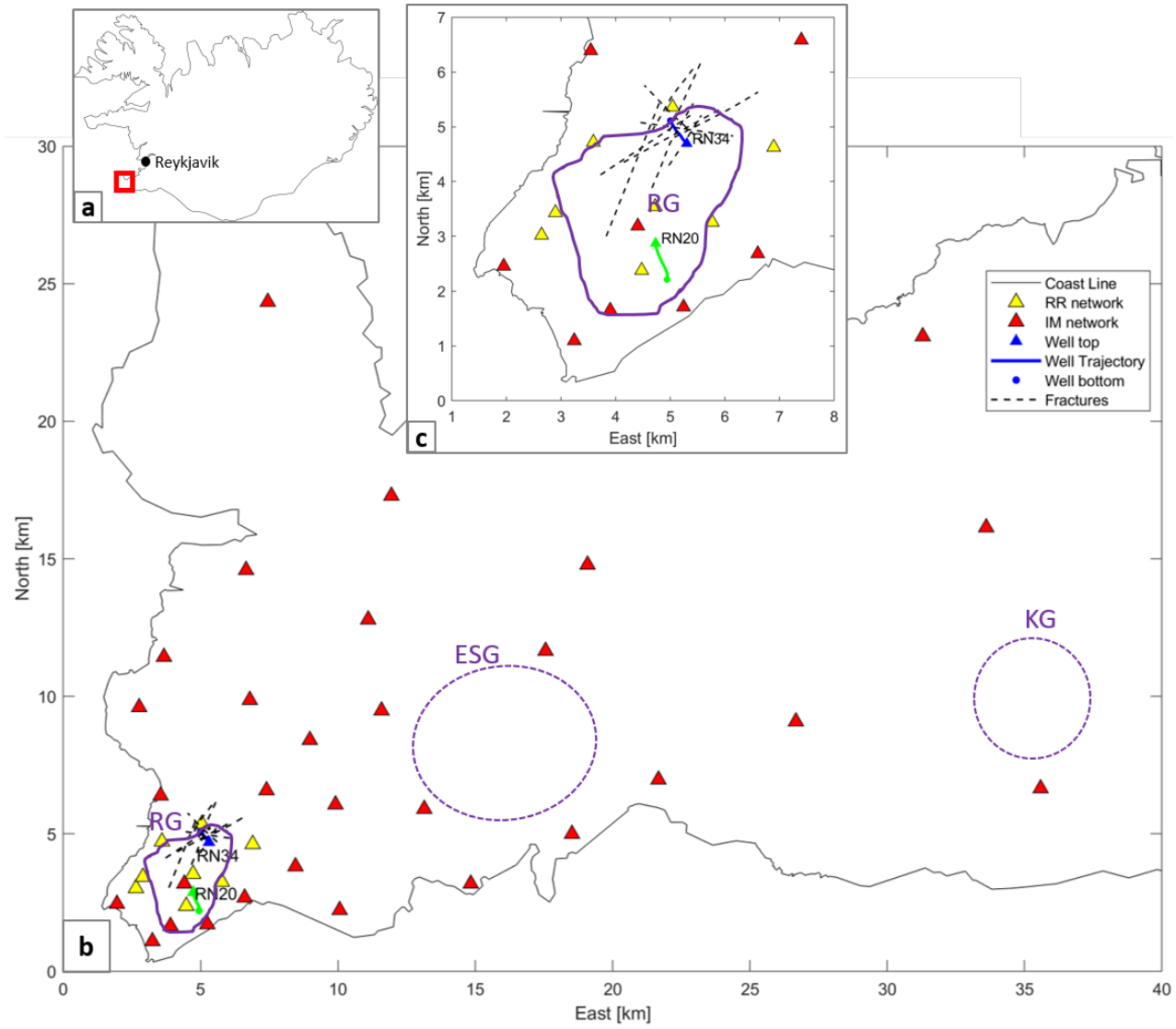

Figure 1: Study area location. (a) Global map of Iceland. The Reykjanes Peninsula, at the South-West of the island, is indicated by a red square whose the size is exaggerated. (b,c) Zooms on the Reykjanes (b) Peninsula and (c) Geothermal field. Red and yellow triangles show the location of the IM and RR sensor networks, respectively. Then, blue and green triangles, lines and dotes indicate the top, trajectory, and the bottom of two injection wells. The black dashed lines represent some known fractures. The approximate locations of the Reykjanes (RG), Eldvörp-Svartsengr (ESG) and Krýsuvík (KG) geothermal fields are indicated by the entire purple contour (RG) and the dashed purple contours (ESG, KG), respectively.

Besides, the Peninsula presents a complex tectonic context as it forms a transition zone from the Reykjanes Ridge (RR) to a transform zone (South Iceland Seismic Zone: SISZ). Therefore, this area is one of the

seismically most active parts of Iceland. Since 1926, periods of increased seismic activity occur every 25-30 years (Keiding et al., 2009), and result in both seismic swarms (on the East part) and mainshock-aftershock sequences (on the West part). The estimated local magnitudes range from about 0 to 6.5 (Keiding et al., 2009). Five active geothermal fields are also located at the intersections between eruptive fissures and transform faults. They induce seismicity in addition to the natural seismicity.

The Reykjanes geothermal field is located at the southern point of the Peninsula, having a size of 1-2 km^2, and has been operational since 2006. Here, we specifically focus on the seismicity occurring during injections from the 20th of May 2015 to the 14th of August 2015.

2.2 The sensor networks and the available seismic data

A 1-D array of 38 three-component surface geophones recorded the seismic activity from April 2014 until August 2015, in the Reykjanes Peninsula (Figure 1.b). This sensor array is split in a permanent and a temporary network, called RR and IM, respectively. The RR sensor network consists of 8 short-period LE-3Dlite geophones, run by ISOR on behalf of the geothermal power plan company HS Orka (Weemstra et al., 2016), and located on the top of the Reykjanes geothermal field. The distance between sensors varies between 0.5 km and 4.2 km with a mean value of 1.5 km between two consecutive stations. As for the IM network, it was deployed in the whole Reykjanes Peninsula, in the context of the European project IMAGE. This network is composed of 30 stations, of which 20 were Trillium Compact Broadband and 10 short-period Mark L-4C seismometers (Jousset et al., 2016). These sensors are further from each other than the RR network sensors as the inter-sensor distance goes from 0.8 km up to 35 km. The use of broadband and short-period geophones allows recording the smallest induced seismic events as well as the biggest natural earthquakes. Moreover, short distances between sensors allow for a better focus on induced seismicity whereas large distances between sensors allow for recording more remoted earthquakes. Consequently, both induced and natural seismicity are recorded well.

During one and a half years of sensor deployment, some stations did not work for short periods of time. This results in some gaps in the continuous seismic data. Consequently, seismicity is recorded by a range of 7 to 38 seismic stations. The 3 weeks (22, 24 and 30) that we focus on in this article have been analyzed in detail, where we check all data, test processing methods and the influence of sensor gaps, and make a first interpretation.

2.3 Injection settings

The injection well was drilled down to 2580 m depth, with an inclination of up to 20° from the vertical. Well logging showed several likely feed points, with the three main features located at a depth of 2380-2580 m. In the period of interest herein, starting 20th of May 2015, fresh water was injected with an estimated rate of 30-35 L/s. Prior to this period, in the first half of April, the well was stimulated by a multistep injection test.

3. METHODS

3.1 Detection and picking

An STA/LTA triggering method applied on the continuous seismic data from the two seismic networks for each week of interest, leads to the detection of about 1800 induced and natural earthquakes. As this study focuses on induced seismic events, a first sorting based on the seismic event waveforms has been done to remove natural seismicity. Therefore, we kept 850 events that are likely to be induced.

These suspected induced events are characterized by a generally low signal-to-noise ratio and the presence of emergent P-waves, but the waveforms show often clear S-onsets. Thus, an accurate identification of P- and S-onsets is challenging. Moreover, a manual identification would require significantly long processing time. This has motivated the development of an automatic picking method based on seismic waveform similarities. P- and S-phases of a representative event (Master Event) are cross-correlated with the entire seismic waveforms of a new event where we want to estimate phase arrivals automatically (Child Event). P- and S- picks of the child event are determined from the time-lags between the traces at which maximum cross-correlation values are observed (Duboeuf et al., 2019). Then, each event is visually inspected to quality control the automatically estimated phase onsets.

3.2 Absolute and Relative Locations

An absolute location has been performed, using a Differential Evolution approach (Storn & Price, 1997; Wuestefeld et al., 2018). This method determines event locations by generating at each step a new population of potential locations. The mean event location misfit decreases at each iteration, allowing to inspect local minima, and at the same time converges to the absolute minimum due to the perturbation of the search space. The stop criterion is based on the difference in the standard deviation of the misfit value of all our populations (Wuestefeld et al. 2018). Using a 1D layered velocity model (SIL, (Bjarnason et al., 1993)), 676 earthquakes have been located, among which 85 % have an average uncertainty of less than 700 m. However, earthquakes occurring on the Reykjanes Ridge are excluded from the following analysis as they are considered to be of tectonic origin and not induced seismicity. Consequently, 626 seismic events were considered hereafter.

Some seismic events visually present waveform similarities. Consequently, all events have been cross-correlated, after we applied a bandpass filter between 2 and 30 Hz. Then, a relative location based on the double difference method (Waldhauser & Ellsworth, 2000) has been performed and leads to the relocation of 537 events. 89 events could not be relocated, and these have

therefore only an absolute event location. Hereafter, we refer to these events as NREs (Non-Relocated Events), whereas REs will refer to relocated events.

3.3 Clustering

Families of similar events, called event clusters, have been created based on both cross-correlation coefficients and double-differential travel-times. Two coefficients CM (Composite Correlation Measure, equation 1) and TM (Composite Time Measure, equation 2) have been defined (Stuermer et al., 2011, 2012). We normalize these parameters such that they vary between 0 and 1.

$$CM_{ij} = \sqrt[2M]{\prod_{k=1}^{M} {}^{P}C_{ij}^{k} \times \prod_{k=1}^{M} {}^{S}C_{ij}^{k}}, \qquad [1]$$

where ${}^{P|S}C_{ij}^{k}$ is the maximum coefficient for event pair ij at station k and for the P- or S- waves and M is the maximum number of sensors.

$$TM_{ij} = \sqrt[M]{\prod_{k=1}^{M}[1 - \frac{\left|({}_{k}t_{i}^{S} - {}_{k}t_{i}^{P}) - ({}_{k}t_{j}^{S} - {}_{k}t_{j}^{P})\right|}{t_{norm}}]}, \qquad [2]$$

where ${}_{k}t_{i}^{S} - {}_{k}t_{i}^{P}$ is the differential travel time between S- and P- phases observed at station k for event i.

The closer CM and TM are to 1, the more similar the event's waveforms are and the closer their event locations are. This method only requires P and S picks in order to compute CM and TM and is therefore independent of the event locations. Then, we gather events in clusters in which the couple (CM; TM) must be greater than (0.6; 0.96). As a result, we obtain 233 events, gathered in 9 clusters.

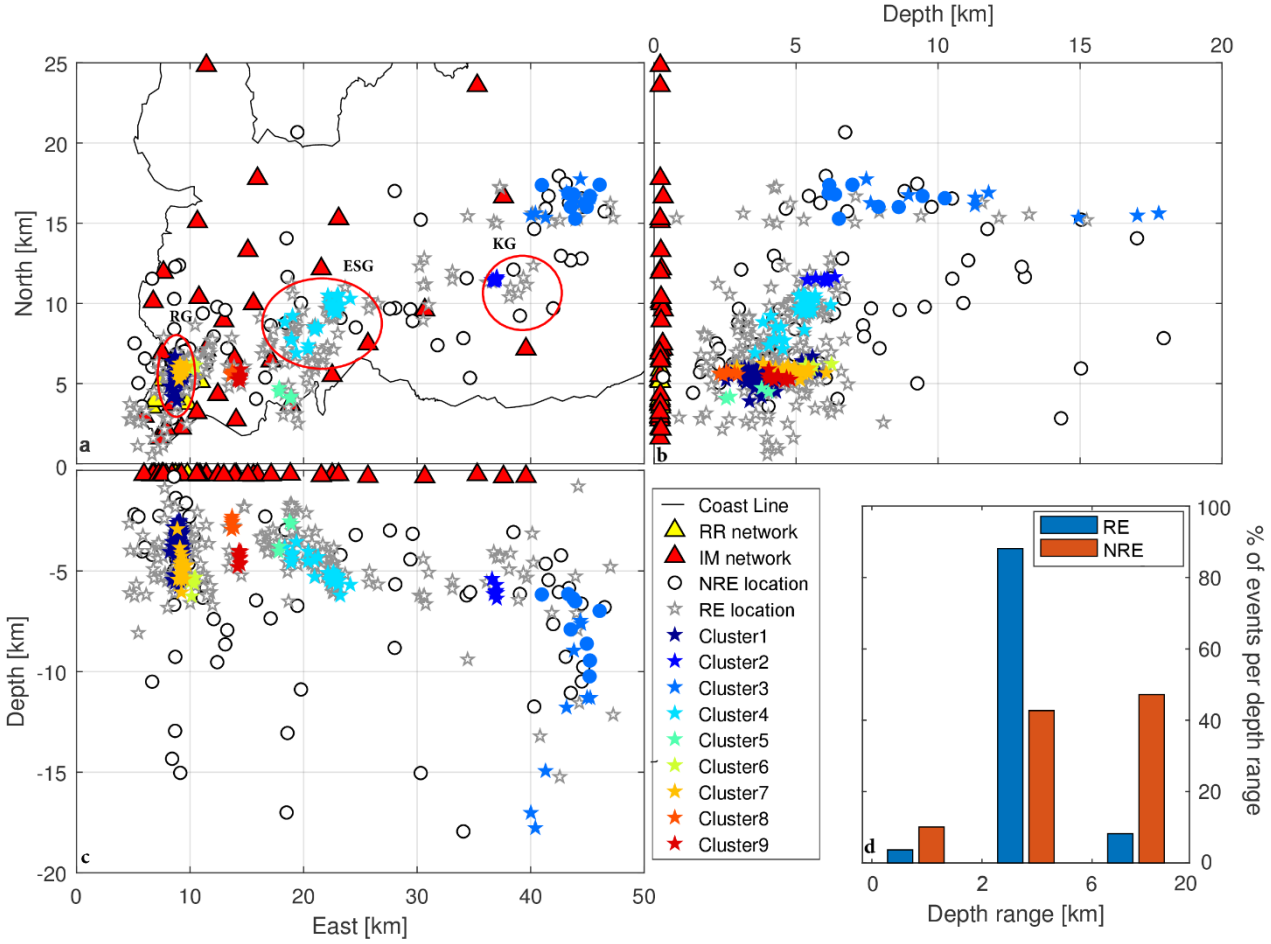

Figure 2: (a,b,c) Absolute and Relative Locations of the detected seismic events in 3D, occurring during the weeks 22, 24 and 30 in 2015. Dots represent the absolute locations of events which have not been relocated whereas the stars symbolize the relative event locations. The colored stars show 9 different event clusters, defined using CM and TM coefficients. The yellow and red triangles indicate the RR and IM networks, respectively. Note that x and y axis have not the same scale. (a) is a 2D horizontal view where the red circles indicate an approximated location of the Reykjanes (RG), Eldvörp-Svartsengr (ESG) and Krýsuvík (KG) geothermal fields, (b) is a 2D East-North view and (c) is a 2D East-Depth view. (d) represents the percentage of the relocated (blue) and non-relocated (orange) seismic events according 3 ranges of depth: [0-2], [2-6] and [6-20] km.

4. RESULTS AND DISCUSSION

4.1 Relocated and Non-Relocated Event (RE and NRE) characteristics

Figure 2.abc presents RE and NRE locations in 3-dimensions. REs form three distinct patches of earthquakes (Figure 2.a) through the Peninsula, whose location in the North-East direction is close to the Reykjanes (RG), Eldvörp-Svartsengr (ESG) and Krýsuvík (KG) geothermal field locations. As for the NREs, they are more scattered on the Peninsula. This location difference between REs and NREs is also observed in depth (Figure 2.d) as 90% of the REs occurred between 2 and 6 km of depth versus only 43 % for the NREs. In fact, 10 % of the NREs are located between the surface and 2 km and 47 % of them are deeper than 6 km. Moreover, except for 10 events, all REs between 2 and 6 km depth are located below RG, ESG and KG geothermal plants (Figure 2.b.c), which suggests that REs could be induced by the geothermal activity. Reinforcing it, most of the observed seismicity occurs below the injection point in the RG field, where the fluid injection is situated at a depth of 2580 m. This constitutes another evidence that REs are induced events. Finally, this range of 2 to 6 km has been observed before and after this study for other induced events in Iceland. Thus, the few events observed in the RG field between December 2008 and May 2009 are in this depth range (Gudhnason, 2014). Similarly, most of the induced seismicity triggered during the drilling of IDDP-2, is observed in this range (Friðleifsson et al., 2018).

Therefore, seismic events which have been relocated (REs) present a different location pattern than events which could not be relocated (NREs). This might mean that for this case, REs are induced events whereas NREs are natural earthquakes, at least for the deepest ones. This hypothesis will be further investigated in the following sections.

4.2 Clustering

Seismic waveforms are defined by the physical process leading to the rupture, but they also strongly depend on the travel path. That is why, when seismic events present similar waveforms, they are considered as located on the same geological structure (Lay & Wallace, 1995). Gathering similar events in families, i.e. performing clustering, could be an interesting tool to map depth fractures or faults.

Nine clusters of events (Figure 2) have been defined, using 233 events. Except for cluster 3 which contains both REs and NREs, clusters consist only of REs. Clusters 1 to 7 are either within or close to geothermal fields, in the North-East direction and in depth. This might mean those events are induced by the geothermal activity. The locations of clusters 8 and 9 are between the RG and ESG geothermal fields. Within the clusters, REs present a vertical alignment suggesting the presence of one or two vertical fractures.
The cluster 3 (close to the KG field) presents a particular pattern compared to other clusters. First, it is composed both by REs and NREs. Additionally, most of these 18 events occurred deeper than 6 km, which could suggest that events are outside of the geothermal field. However, because of the sensor network distribution, localization is poorly constrained both in depth and in the North-East direction as no sensor is on the eastern side of the cluster. In fact, most of these events present a location uncertainty larger than 500 m in depth whereas all other clusters have significantly smaller uncertainties. Removing those events from this analysis leads to remove almost 10 REs in the deepest part of the Peninsula and reinforces the hypothesis that REs mostly occur above 6 km of depth.

Now, we focus on the Reykjanes geothermal field in which 3 clusters (1, 6 and 7) are identified. Cluster 7 is the deepest one. Events present a quasi-vertical alignment, which could suggest the presence of a vertical fracture. Identically, cluster 6, whose events are aligned between 6 and 4 km (more one event at 3 km), could indicate a vertical fracture in the geothermal field. Finally, cluster 1 is the biggest one and its events are located from 6 to 3 km depth. A sub-clustering of this cluster could be planned to discriminate smallest geological structures.

4.3 Magnitude

Moment magnitudes have been determined fitting a Brune-shaped spectrum to the observed S-wave displacement spectra (Brune, 1970). Before fitting the spectra, the data were corrected for geometrical spreading, intrinsic attenuation (using Qs of 180) and assuming a mean radiation pattern. The resulting moment magnitudes vary between -0.8 and 2.8 (Figure 3). Only 39 events present a moment magnitude greater than 1. Generally, they are the deepest events as 67% of the events larger than M1 occur bellow 6 km depth. None of the events larger than M1 is observed between the surface and 2 km of depth and only one event is located close to 2.1 km depth. The smallest events (Mw < 0) are mainly close to the surface and only few of them are found at greater depths. This might be due to the magnitude of completeness, which is 0.6 (Figure 3.b) and decreasing with larger distance. Thus, events with a magnitude smaller than 0.6 are not always detected.

The comparison of event magnitudes from the REs or NREs highlights a different scheme. REs present a similar magnitude-depth distribution as the whole event dataset (Figure 3.c). On the other hand, most of the biggest magnitude events are also the deepest events. These ones are NREs (Figure 3.d), which suggests that REs and NREs are released by different physical processes. This reinforces the previous hypothesis that REs are induced and NREs are natural. Note that none of the clustered events (Figure 3.e) have a magnitude smaller than 0. This could be due to the cross-correlation computation. The smaller the events are, the bigger the noise is. Even if a filter is applied, this could reduce cross-correlation coefficients and prevent the addition of the smallest events in any clusters.

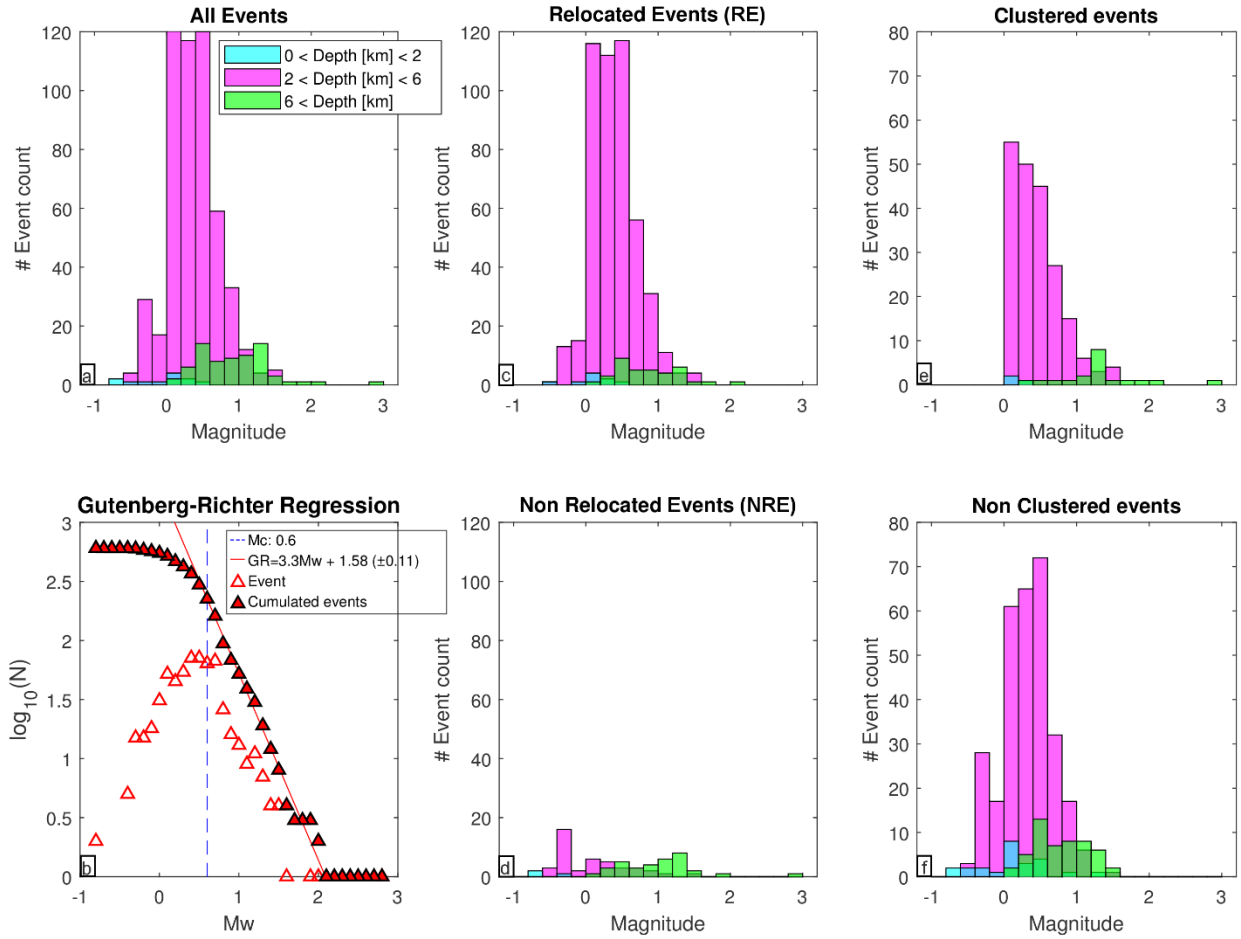

Figure 3: Magnitude study according different parameters. Magnitude evolution in function of (a, c, d, e, f) depth for all, relocated, non-relocated, clustered and non-clustered events, respectively; b) Is the Gutenberg- Richter on the whole dataset.

Following the Gutenberg-Richter law between the event magnitudes and their frequency of occurrence, we compute a b-value of 1.58 (± 0.11). This is unusually high compared to the globally observed b-value for tectonic earthquakes of about 1. However, high b-values have been previously observed in many cases of fluid injections (Shapiro et al., 2013). For instance, Eaton et al. (2014) computed b-values of 1.61, 2.44 and 1.63 for Cotton Valley, Central Alberta and Horn River Basin fields respectively. They explained these high b-values with the high stratification of the studied reservoirs, such that smaller events would occur even more frequently than larger events. In our case, the high b-value could be explained by a lack of big events. Their absence might be due to the length of fracture ruptures. The reactivated fracture could “break” small section by small section rather than only one rupture on the total fracture length. This is supported by the location pattern in function of time (Figure 4) as events appear clustered in time. Another explanation to the lack of big events might be the fluid perturbation size. If fluid perturbation is too small, some magnitudes may not be reached according to McGarr (2014).

4.4 Time

The Reykjanes geothermal field is the most instrumented area of the Peninsula with 23 stations in a 5 km radius around it. This results in a better data resolution, so in a best event location and a reduced location uncertainty. Hence, we restrain the spatial area of our study to this field. Moreover, 183 events of the 354 occurring during week 30 are located in the Reykjanes geothermal field. Among them, only 14 events are NREs. The 95 remaining events not only are REs but also part of one of the 3 clusters. The moment magnitude ranges from -0.8 to 1.6 and the events follow a Gutenberg-Richter law with an estimated b-value of 1.37 and a magnitude of completeness of 0.2. This smaller b-value indicates a more complete event catalogue than when using the whole database. Moreover, more smallest events are included as the magnitude of completeness is smaller. Consequently, this week is representative of the three others. Hereafter, we only focus our analysis on the induced seismicity occurring during the week 30 and in the Reykjanes Geothermal field (Figure 4).

Figure 4.abc presents a 3D view of the seismicity occurring during week 30 as a function of time and as a function of magnitude. As previously noted, the largest events are deeper than the smallest ones. Therefore, an interesting time pattern is observed both at surface and in depth on Figure 4abc. A migration from the depth towards the surface occurred as well as

a migration from the NE towards the SW. Thus, events migrated from the depth North-East to the surface South-West through the seven days of the week 30. Moreover, events from day 1 (Figure 4) with light blue contours are a part of cluster 6 (Figures 2 and 4). This suggests that those events should be located on the same geological structure. This is reinforced by the clustering in time shown in the Figure 4d where events only occur during short periods. Consequently, a vertical fracture is suspected at the location of the events from cluster 6. Afterwards, about half of the events occurring during the days 2 to 7 are from the cluster 1 (Figures 2 and 4). As those events are part of the same cluster, we should think they are on the same structure. Then, this structure should crack in different small sections, as suggested by the high b-value (section 5.c). However, the extension of the event cloud (~700 m) as well as NE-SW and depth-surface migrations do not validate this hypothesis. Part of a same cluster could also be interpreted as events occurring on different structures but with the same physical properties and close to each other. As a clustering time (Figure 4d) is also observed for these events, we propose that the cluster illuminates a set of several parallel fractures, oriented NW-SE, potentially with a dip of about 70 degrees.

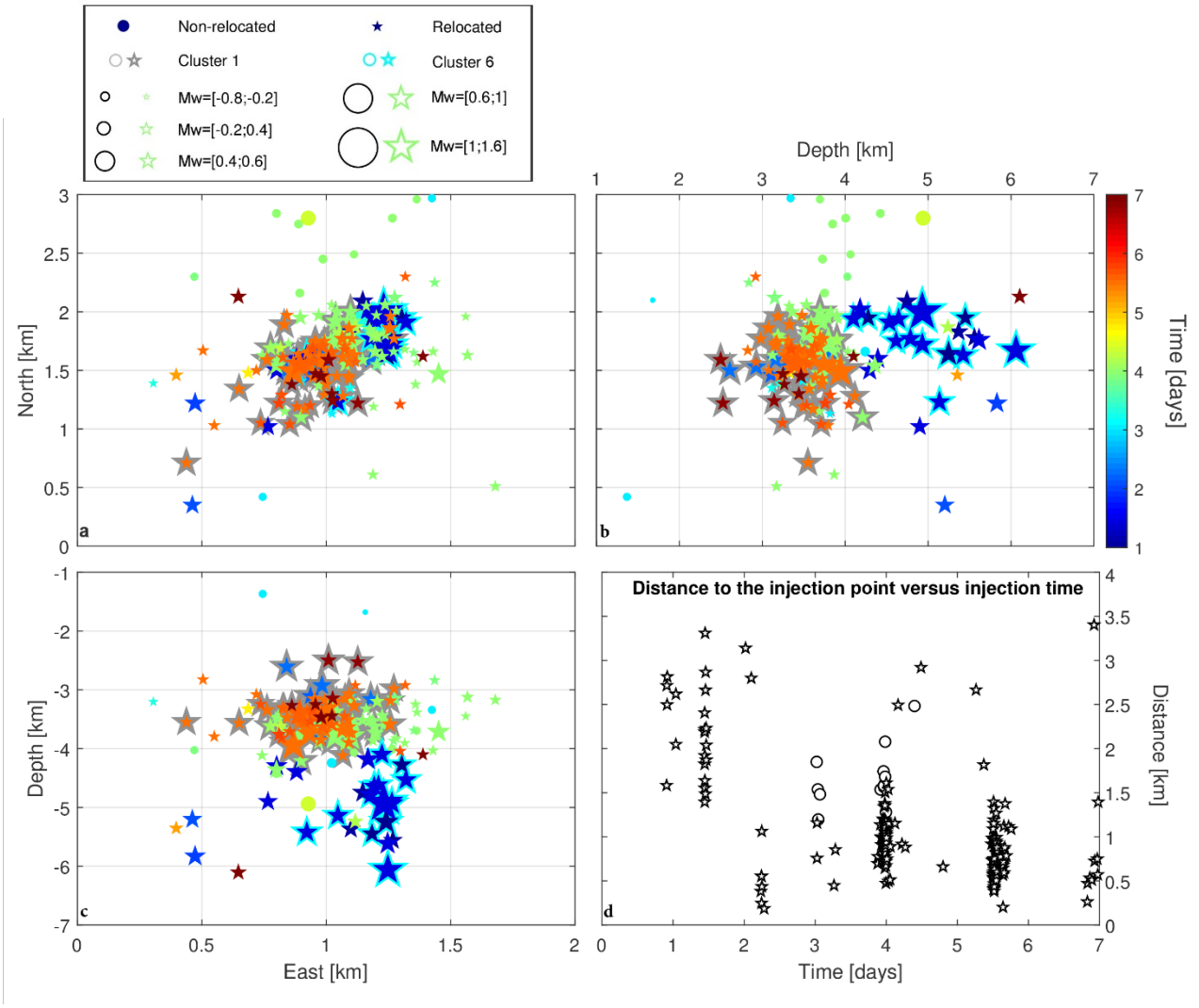

Figure 4: Event locations evolution in function of time and magnitude for the week 30, zoom on the Reykjanes geothermal field. (a) and (b) present a 2D East-North- view and (c) a 2D East-Depth view. Stars indicate relocated events whereas dots show the non-relocated events. Colors from blue to red is the time from the day 1 to day 7 of the week 30. Note that the North, East and Depth scales are not the same. (d) shows distance to the injection point as a function of time (in days). Stars and circles indicate relocated and non-relocated events, respectively.

5. CONCLUSION

Analysis of 626 induced events in the Reykjanes Peninsula highlighted differences in seismic behavior between events that were relocated and others that were non-relocated (RE or NRE). This might be used to make a distinction between induced (RE) and natural (NRE) events. Thus, 537 seismic events were considered as induced. Then, nine clusters of events were identified based on the inter-event distances and their cross-correlation coefficients in order to identify different geological structures. Cluster locations could be outside or inside known geothermal fields,

suggesting the presence of different geological structures. The magnitude computation and more particularly the Gutenberg-Richter law show a lack of big events. This can be interpreted either as a too small fluid perturbation to reach greater magnitude or as several reactivations of the same fracture or a partial reactivation of the fracture rather than only one crack on the whole fracture length. Finally, a joined interpretation of the relocated and clustered events in relation with the magnitude and the time leads us to suspect the presence of one vertical fracture between 6 and 4 km depth in the Reykjanes Geothermal field, and the presence of a set of sub-parallel fractures NE-SW dipping about 70 degrees. These results will then be analyzed together with geological interpretation as well as the computation of focal mechanisms.

REFERENCES

Albaric, J., Oye, V., Langet, N., Hasting, M., Lecomte, I., Iranpour, K., et al. (2014). Monitoring of induced seismicity during the first geothermal reservoir stimulation at Paralana, Australia. *Geothermics*. https://doi.org/10.1016/j.geothermics.2013.10.013

Bachmann, C. E., Wiemer, S., Woessner, J., & Hainzl, S. (2011). Statistical analysis of the induced Basel 2006 earthquake sequence: introducing a probability-based monitoring approach for Enhanced Geothermal Systems. *Geophysical Journal International*, *186*(2), 793. https://doi.org/10.1111/j.1365-246X.2011.05068.x

Bjarnason, I. T., Menke, W., Flóvenz, Ó. G., & Caress, D. (1993). Tomographic image of the Mid-Atlantic Plate Boundary in southwestern Iceland. *Journal of Geophysical Research: Solid Earth*, *98*(B4), 6607–6622. https://doi.org/10.1029/92JB02412

Björnsson, S., & Einarsson, P. (1974). Seismicity of Iceland. In L. Kristjansson (Ed.), *Geodynamics of Iceland and the North Atlantic Area* (pp. 225–239). Dordrecht: Springer Netherlands.

Brodsky, E. E., & Lajoie, L. J. (2013). Anthropogenic Seismicity Rates and Operational Parameters at the Salton Sea Geothermal Field. *Science*, *341*(6145), 543–546. https://doi.org/10.1126/science.1239213

Brune, J. N. (1970). Tectonic stress and the spectra of seismic shear waves from earthquakes. *Journal of Geophysical Research*, *75*(26), 4997–5009. https://doi.org/10.1029/JB075i026p04997

Cornet, F. H. (2016). Seismic and aseismic motions generated by fluid injections. *Geomechanics for Energy and the Environment*, *5*, 42–54. https://doi.org/http://dx.doi.org/10.1016/j.gete.2015.12.003

Cornet, F. H., Helm, J., Poitrenaud, H., & Etchecopar, A. (1997). Seismic and Aseismic Slips Induced by Large-scale Fluid Injections. In S. Talebi (Ed.), *Seismicity Associated with Mines, Reservoirs and Fluid Injections* (pp. 563–583). Basel: Birkhäuser Basel. https://doi.org/10.1007/978-3-0348-8814-1_12

Cornet, F. H., Bérard, T., & Bourouis, S. (2007). How close to failure is a granite rock mass at a 5km depth? *International Journal of Rock Mechanics and Mining Sciences*, *44*(1), 47–66. https://doi.org/https://doi.org/10.1016/j.ijrmms.2006.04.008

Cuenot, N., Dorbath, C., & Dorbath, L. (2008). Analysis of the Microseismicity Induced by Fluid Injections at the EGS Site of Soultz-sous-Forêts (Alsace, France): Implications for the Characterization of the Geothermal Reservoir Properties. *Pure and Applied Geophysics*, *165*(5), 797–828. https://doi.org/10.1007/s00024-008-0335-7

Deichmann, N., & Giardini, D. (2009). Earthquakes Induced by the Stimulation of an Enhanced Geothermal System below Basel (Switzerland). *Seismological Research Letters*, *80*(5), 784–798. https://doi.org/10.1785/gssrl.80.5.784

Duboeuf, L., Oye, V., Berre, I., Keilegavlen, E., & Dando, B. (2019). Automatic picking for induced seismicity in Iceland using an EAT (Empirically Aggregated Template) methodology. In *Schatzalp workshop 2019*.

Eaton, D. W., Davidsen, J., Pedersen, P. K., & Boroumand, N. (2014). Breakdown of the Gutenberg-Richter relation for microearthquakes induced by hydraulic fracturing: influence of stratabound fractures. *Geophysical Prospecting*, *62*(4), 806–818. https://doi.org/10.1111/1365-2478.12128

Fehler, M., Jupe, A., & Asanuma, H. (2001). More than cloud: New techniques for characterizing reservoir structure using induced seismicity. *The Leading Edge*, *20*(3), 324–328.

Friðleifsson, G. Ó., Elders, W. A., Zierenberg, R. A., Fowler, A. P. G., Weisenberger, T. B., Mesfin, K. G., et al. (2018). The Iceland Deep Drilling Project at Reykjanes: Drilling into the root zone of a black smoker analog. *Journal of Volcanology and Geothermal Research*. https://doi.org/10.1016/J.JVOLGEORES.2018.08.013

Gudhnason, E. Á. (2014). *Analysis of seismic activity on the western part of the Reykjanes Peninsula, SW Iceland, December 2008-May 2009*.

Jakobsdóttir, S. S. (2008). Seismicity in Iceland: 1994--2007. *Jökull*, *58*, 75–100.

Jousset, P., Blanck, H., Franke, S., Metz, M., Ágústsson, K., Verdel, A., et al. (2016). Seismic tomography in Reykjanes, SW Iceland. *Extended Abstract EGC, Strasbourg*.

Keiding, M., Lund, B., & Árnadóttir, T. (2009). Earthquakes, stress, and strain along an obliquely divergent plate boundary: Reykjanes Peninsula, southwest Iceland. *Journal of Geophysical Research: Solid Earth*, *114*(B9).

Khodayar, M., Björnsson, S., Gudhnason, E. Á., Nielsson, S., Axelsson, G., & Hickson, C. (2018). Tectonic Control of the Reykjanes Geothermal Field in the Oblique Rift of SW Iceland: From Regional to Reservoir Scales. *Open Journal of Geology*, *8*(03), 333.

Kwiatek, G., Martínez-Garzón, P., Dresen, G., Bohnhoff, M., Sone, H., & Hartline, C. (2015). Effects of long-term fluid injection on induced seismicity parameters and maximum magnitude in northwestern part of The Geysers geothermal field. *Journal of Geophysical Research: Solid Earth*, *120*(10), 7085–7101. https://doi.org/10.1002/2015JB012362

Lay, T., & Wallace, T. C. (1995). Body Waves and Ray Theory. *International Geophysics*, *58*, 70–115. https://doi.org/10.1016/S0074-6142(05)80004-X

Li, Y., Cheng, C. H., & Toksöz, M. N. (1998). Seismic monitoring of the growth of a hydraulic fracture zone at Fenton Hill, New Mexico. *Geophysics*, *63*(1), 120–131.

Martínez-Garzón, P., Bohnhoff, M., Kwiatek, G., & Dresen, G. (2013). Stress tensor changes related to fluid injection at The Geysers geothermal field, California. *Geophysical Research Letters*, *40*(11), 2596–2601. https://doi.org/10.1002/grl.50438

McGarr, A. (2014). Maximum magnitude earthquakes induced by fluid injection. *Journal of Geophysical Research: Solid Earth*, *119*(2), 1008–1019. https://doi.org/10.1002/2013JB010597

Michelet, S., & Toksöz, M. N. (2007). Fracture mapping in the Soultz-sous-Forêts geothermal field using microearthquake locations. *Journal of Geophysical Research: Solid Earth*, *112*(B7).

Phillips, W. S., House, L. S., & Fehler, M. C. (1997). Detailed joint structure in a geothermal reservoir from studies of induced microearthquake clusters. *Journal of Geophysical Research: Solid Earth*, *102*(B6), 11745–11763.

Rowe, C. A., Aster, R. C., Phillips, W. S., Jones, R. H., Borchers, B., & Fehler, M. C. (2002). Using automated, high-precision repicking to improve delineation of microseismic structures at the Soultz geothermal reservoir. In *The Mechanism of Induced Seismicity* (pp. 563–596). Springer.

Schmittbuhl, J., Lengliné, O., Cornet, F. H., Cuenot, N., & Genter, A. (2014). Induced seismicity in EGS reservoir: the creep route. *Geothermal Energy*, *2*(1), 1–13. https://doi.org/10.1186/s40517-014-0014-0

Shapiro, S. A., Audigane, P., & Royer, J.-J. (1999). Large-scale in situ permeability tensor of rocks from induced microseismicity. *Geophysical Journal International*, *137*(1), 207–213. https://doi.org/10.1046/j.1365-246x.1999.00781.x

Shapiro, S. A., Rothert, E., Rath, V., & Rindschwentner, J. (2002). Characterization of fluid transport properties of reservoirs using induced microseismicity. *Geophysics*, *67*(1), 212–220. https://doi.org/10.1190/1.1451597

Shapiro, S. A., Krüger, O. S., & Dinske, C. (2013). Probability of inducing given-magnitude earthquakes by perturbing finite volumes of rocks. *Journal of Geophysical Research: Solid Earth*, *118*(7), 3557–3575. https://doi.org/10.1002/jgrb.50264

Storn, R., & Price, K. (1997). Differential evolution--a simple and efficient heuristic for global optimization over continuous spaces. *Journal of Global Optimization*, *11*(4), 341–359.

Stuermer, K., Kummerow, J., & Shapiro, S. A. (2011). Waveform Similarity Analysis at Cotton Valley, Texas. In *SEG Technical Program Expanded Abstracts 2011* (pp. 1669–1673). Society of Exploration Geophysicists.

Stuermer, K., Kummerow, J., & Shapiro, S. A. (2012). Multiplet based extraction of geological structures. In *SEG Technical Program Expanded Abstracts 2012* (pp. 1–5). Society of Exploration Geophysicists.

Thordarson, T., & Larsen, G. (2007). Volcanism in Iceland in historical time: Volcano types, eruption styles and eruptive history. *Journal of Geodynamics*, *43*(1), 118–152. https://doi.org/10.1016/J.JOG.2006.09.005

Waldhauser, F., & Ellsworth, W. L. (2000). A Double-Difference Earthquake Location Algorithm: Method and Application to the Northern Hayward Fault, California. *Bulletin of the Seismological Society of America*, *90*(6), 1353–1368. https://doi.org/10.1785/0120000006

Weemstra, C., Obermann, A., Verdel, A., Paap, B., Blanck, H., Gunason, E. Á., et al. (2016). Time-lapse seismic imaging of the Reykjanes geothermal reservoir. In *Proceedings of the European Geothermal Congress. European Geothermal Energy Council (EGEC), Strassbourg*.

Wei, S., Avouac, J.-P., Hudnut, K. W., Donnellan, A., Parker, J. W., Graves, R. W., et al. (2015). The 2012 Brawley swarm triggered by injection-induced aseismic slip. *Earth and Planetary Science Letters*, *422*, 115–125. https://doi.org/http://dx.doi.org/10.1016/j.epsl.2015.03.054

Wuestefeld, A., Greve, S. M., Näsholm, S. P., & Oye, V. (2018). Benchmarking earthquake location

algorithms: A synthetic comparison. *Geophysics*, *83*(4), KS35--KS47.

Zhang, Q., Lin, G., Zhan, Z., Chen, X., Qin, Y., & Wdowinski, S. (2017). Absence of remote earthquake triggering within the Coso and Salton Sea geothermal production fields. *Geophysical Research Letters*, *44*(2), 726–733. https://doi.org/10.1002/2016GL071964

Acknowledgements

We thank the Research Council of Norway for funding through the ERiS project, grant #267908, and ÍSOR (Iceland) for the data access.